Application of Linear-Frequency-Modulated Continuous-Wave (LFMCW) Radars for Tracking of Vital Signs

Guochao Wang, *Student Member, IEEE*, José-María Muñoz-Ferreras, Changzhan Gu, *Member, IEEE*, Changzhi Li, *Senior Member, IEEE*, and Roberto Gómez-García, *Senior Member, IEEE*

***Abstract*—This paper focuses on the exploitation of linear-frequency-modulated continuous-wave (LFMCW) radars for noncontact range tracking of vital signs, e.g., respiration. Such short-range system combines hardware simplicity and tracking precision, thus outperforming other remote-sensing approaches in the addressed biomedical scenario. A rigorous mathematical analysis of the operating principle of the LFMCW radar in the context of vital-sign monitoring, which includes the explanation of key aspects for the maintenance of coherence, is detailed. A precise phase-based range-tracking algorithm is also presented. Exhaustive simulations are carried out to confirm the suitability and robustness against clutter, noise, and multiple scatterers of the proposed radar architecture, which is subsequently implemented at the prototype level. Moreover, live data from real experiments associated to a metal plate and breathing subjects are obtained and studied.**

***Index Terms*—Biomedical applications, linear-frequency-modulated continuous-wave (LFMCW) radars, range tracking, short-range radars, vital signs, wireless sensors.**

I. Introduction

MONITORING of vital signs has recently attracted the attention of radar researchers (see [1] and [2] and the references therein). Different target motions along the radar line-of-sight (LOS) give rise to different Doppler frequencies, which constitute the so-called "micro-Doppler" features of the target [3], [4]. They can be used, for instance, for classification purposes. Examples encompass the utilization of this Doppler information together with the range signature to form an inverse-synthetic-aperture-radar (ISAR) image, which can be exploited to analyze the human gait or to classify helicopters [5]–[7].

In the healthcare context, radars have become an interesting approach to monitor vital signs—mainly heartbeats and respiration patterns—without contact. The emerging scenarios of application are manifold, including the following: monitoring of sudden infant death syndrome or of adult sleep apnea, acquisition of lung function measurements, assessment of key parameters in relation with cardiopulmonary activity or for a more efficient employment of radiotherapy, observation of children subject to hyperthermia when left unattended in a car, and other new applications [2], [8]–[11].

In the aforementioned biomedical background, two mainstreams for radar architectures can be found in the technical literature with their corresponding benefits and shortcomings. They are as follows:

- Doppler radars [12]–[18];
- impulse-radio ultra-wideband (IR-UWB) radars [2], [19]–[23].

On the one hand, Doppler radars operate by emitting a single tone to obtain the phase history—and hence, the Doppler information—of a moving target. As a consequence, they are single-tone continuous-wave (CW) radars. Since they do not transmit an instantaneous bandwidth, they do not possess range resolution. This leads to a poor range isolation of the desired target from surrounding clutter, thus degrading the capability of tracking small motions of the wanted target. Furthermore, these Doppler radars are subject to problems related to dc offsets and in-phase/quadrature (I/Q) imbalances, which largely complicate their architectures to compensate their effects. These schemes are novel and very valuable, but are not simple. A very interesting advantage of these CW radar systems is the fact that range tracking is based on phase measurements, which confers a high precision upon them.

On the other hand, IR-UWB radars transmit a large bandwidth, which enables a very high-range resolution to be achieved. This is accomplished through the emission of very temporarily narrow radio impulses. Not very strong signal-energy levels can be then transmitted, thus reducing the signal-to-noise ratio (SNR), and hence, compromising the precision. Moreover, the range-tracking algorithm is not based on phase measurements. Note that phase usage is convenient to get high precision, despite possible ambiguities that could arise. IR-UWB radars use very innovative schemes to ac-

Manuscript received October 24, 2013; revised January 02, 2014 and April 11, 2014; accepted April 21, 2014. Date of publication May 05, 2014; date of current version June 02, 2014. This work was supported in part by the University of Alcalá under Project CCG2013/EXP-038 and the National Science Foundation under Grant ECCS-1254838 and Grant CMMI-1131506.

G. Wang and C. Li are with the Department of Electrical and Computer Engineering, Texas Tech University, Lubbock, TX 79409 USA (e-mail: guochao.wang@ttu.edu; changzhi.li@ttu.edu).

C. Gu was with the Department of Electrical and Computer Engineering, Texas Tech University, Lubbock, TX 79409 USA. He is now with MaxLinear Inc., Irvine, CA 92618 USA (e-mail: changzhan.gu@ttu.edu).

J.-M. Muñoz-Ferreras and R. Gómez-García are with the Department of Signal Theory and Communications, University of Alcalá, Polytechnic School, Alcalá de Henares 28871, Madrid, Spain (e-mail: jm.munoz@uah.es; roberto.gomez.garcia@ieee.org).

Color versions of one or more of the figures in this paper are available online at http://ieeexplore.ieee.org.

Digital Object Identifier 10.1109/TMTT.2014.2320464

quire such narrow pulses, but again these architectures are far from simple. In any case, it is unquestionable that they have demonstrated excellent capabilities for different biomedical remote-sensing purposes, such as heartbeat monitoring and tracking of more-than-one person in static and mobile scenarios.

In this paper, which extends a preliminary work of the authors, pure linear-frequency-modulated continuous-wave (LFMCW) radars are proposed for healthcare applications [24]. Other approaches with combined single-tone CW and LFMCW waveforms, hence exploiting a different operation philosophy, can be found in the technical literature [25], [26]. For example, this hybrid waveform was employed in a self-injection-locked radar in [25]. Here, the suggested pure LFMCW radar configuration is halfway between Doppler and IR-UWB radars as an attempt to overcome their drawbacks. Firstly, it transmits a finite bandwidth to isolate the target from surrounding clutter. Secondly, it uses the phase to get enhanced precision in range tracking. Thirdly, since it is a CW radar, more signal energy can be transmitted and an improved SNR can thus be attained.

The operating principle of an LFMCW radar for vital-sign monitoring is reported here. Special emphasis is made on concepts related to range resolution and coherence maintenance as key issues to properly extract the phase history of the illuminated target. Simulated data along with a robustness analysis against clutter and noise are provided. Although simulations assume a point scatterer as proof-of-concept, more sophisticated scenarios consisting of multiple in-phase moving scatterers to model more realistic situations are also addressed. This radar architecture is experimentally validated through a prototype, which is employed to capture real-experiment live data coming from a metal plate and breathing subjects. The obtained measured results permit to corroborate the aforementioned mathematical framework and simulations.

This paper is organized as follows. Section II expounds the theoretical foundations of LFMCW radars in the context of vital-sign monitoring. The algorithm to extract the range history of the target is also derived here. Exhaustive simulations to confirm the suitability of this radar approach are reported in Section III. After the description of a developed LFMCW radar prototype for verification, real experimental then results corresponding to a vibrating metal plate and breathing subjects are presented in Section IV. Finally, the main conclusions of this work are set out in Section V.

II. Operating Principle of LFMCW Radars for Vital-Sign Monitoring

Due to continuous operation of CW radars, the receiver (Rx) must be switched on during transmitter (Tx) emissions. The transmitted high-power signal levels can easily degrade the Rx sensitivity, and thus, strict isolation requirements are necessary. Hence, the conventional pulsed-radar scheme with an isolator, such as the one shown in Fig. 1(a), is usually avoided in CW radars. In contrast, two directive antennas to increase the Tx–Rx isolation are normally used as depicted in Fig. 1(b).

As commented in Section I, Doppler radars, such as the police radar [27], can obtain the speed of a single illuminated target by means of the Doppler effect. However, they cannot extract the absolute range of the target. In vital-sign monitoring, the phase history can be derived and related to the relative range evolution, but no absolute range information can be obtained. Note that range resolution ΔR is a key issue to isolate different targets in range. It depends on the instantaneous transmitted bandwidth B as the following formula indicates:

$$\Delta R = \frac{c}{2B} \tag{1}$$

where c is the speed of light [28], [29].

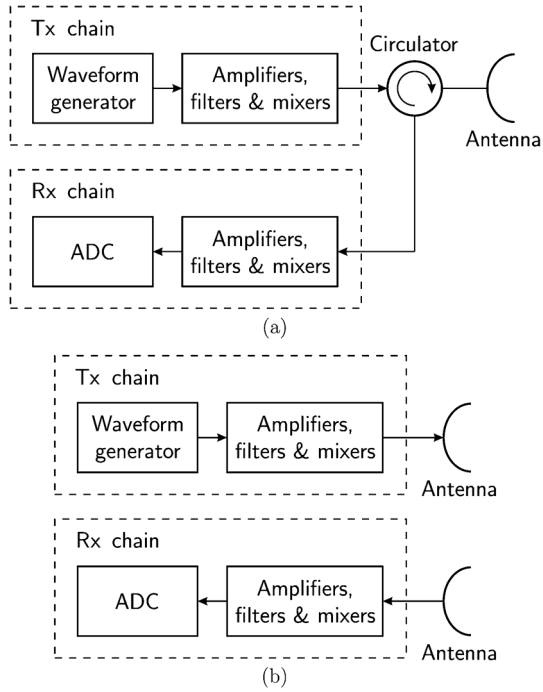

Fig. 1. Conventional architectures for a radar system (analog-to-digital converter: ADC). (a) Circulator + single-antenna solution: pulsed radars. (b) Tx- and Rx-antenna solution: CW radars.

As previously mentioned, CW radars continuously transmit a signal. This means that the energy received from the target is large when compared to that received by a pulsed radar, where the peak power is usually limited [28], [29]. The SNR is then better, which ultimately leads to a finer precision. In addition to this benefit, an LFMCW radar possesses range resolution. Fig. 2 depicts the instantaneous frequency of the LFMCW waveform, where B is the transmitted bandwidth, PRF is the ramp repetition frequency,[1] and f_c is the center frequency [30].

The mathematical expression for the transmitted complex analytic signal for one waveform period can be formulated as

$$s_{\mathrm{Tx}}(t) = \exp\left(j(2\pi f_c t + \pi\gamma t^2 + \phi)\right). \tag{2}$$

In the above equation, $\gamma = B \cdot \mathrm{PRF}$ corresponds to the chirp rate—i.e., the instantaneous-frequency slope in Fig. 2—ϕ is the initial phase, and t is the so-called "fast-time" for the interval $[-T/2, T/2]$ where $T = \mathrm{PRF}^{-1}$ [24].

Imagine a point scatterer whose distance to the LFMCW radar sensor varies as modeled by $R(\tau)$, where τ is the so-called

[1]PRF classically refers to "pulse repetition frequency," a concept extensively used for pulsed radars. Here, this terminology is maintained for historical reasons.

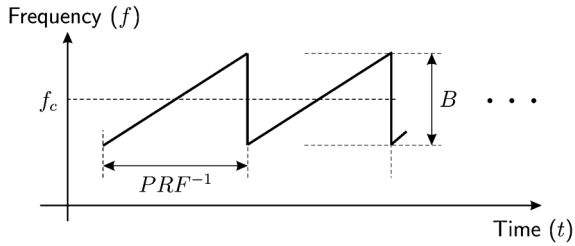

Fig. 2. Instantaneous frequency of the waveform for an LFMCW radar.

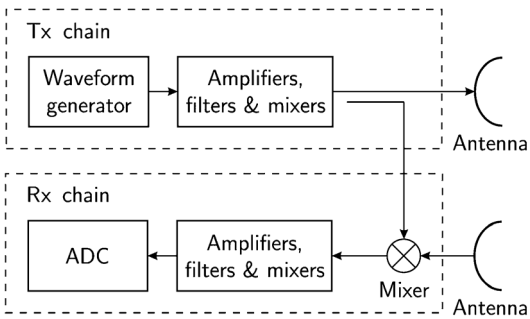

Fig. 3. Deramping-based architecture for an LFMCW radar.

"slow-time." The range $R(\tau)$ can be assumed to be constant during each period of the transmitted waveform [31]. This "stop-and-go" hypothesis is a very good approximation for slow targets—such as the ones considered in this work—and noticeably simplifies the next analysis.[2] The formula for the received signal for this point scatterer at $R(\tau)$ is given by

$$s_{\mathrm{Rx}}(t) = \sigma s_{\mathrm{Tx}}\left(t - \frac{2R(\tau)}{c}\right) \tag{3}$$

where σ is the amplitude of this signal, which comes mainly influenced by two parameters: the target radar cross section (RCS) and the propagation losses.

After an I/Q demodulation, the received signal of (3) can be acquired by an ADC, as shown in Fig. 1(b). To handle the large-signal bandwidth—hundreds of megahertz—usually required to achieve high-range resolution [32], a high-demanding acquisition system is necessary. To circumvent this problem, the scheme of Fig. 1(b) can be replaced by the deramping-based architecture of Fig. 3. This analog deramping procedure, also known as "dechirping," basically consists of mixing a replica of the transmitted signal of (2) with the received one of (3) [33]. At the mixer output, the deramping process produces the so-called "beat signal," which is much easier to acquire as demonstrated below.

The mathematical expression for the beat signal within the interval $t \in [-T/2, T/2]$ is ($(\cdot)^*$ denotes the complex-conjugate operation)

$$\begin{aligned} s_b(t) &= s_{\mathrm{Tx}}(t)s^*_{\mathrm{Rx}}(t) \\ &= \sigma \exp\left(j\left(\frac{4\pi\gamma R(\tau)t}{c} + \frac{4\pi f_c R(\tau)}{c} + \phi_2\right)\right). \end{aligned} \tag{4}$$

[2]The violation of the "stop-and-go" assumption gives rise to unexpected effects, such as those observed for the high-speed blades of a helicopter [7].

As inferred from (4), a single point scatterer generates a sinusoidal beat signal whose frequency is

$$f_b = \frac{2\gamma R(\tau)}{c}. \tag{5}$$

Additionally, the phase $4\pi R(\tau) f_c/c$ is the standard slow-time phase history, and the third term in (4) ($\phi_2 = -4\pi\gamma R^2(\tau)/c^2$) is the residual video phase (RVP), which is found to be negligible and can then be ignored [31].

According to (5), the beat signal exhibits a frequency, which is proportional to the point-scatterer range. This means that the distance information is contained in the frequency domain. In fact, if a Fourier transform is performed over each period of the beat signal, its associated range profile is derived. This fast-time Fourier transform $S_b(f)$ can be shown to be

$$S_b(f) = \sigma T \exp\left(j\frac{4\pi f_c R(\tau)}{c}\right) \mathrm{sinc}\left(T\left(f - \frac{2\gamma R(\tau)}{c}\right)\right) \tag{6}$$

where $\mathrm{sinc}(x) = \sin(\pi x)/(\pi x)$. After a simple scaling process of the frequency axis, the corresponding range profile can be extracted. It should be noticed that the range width of the sinc function is equal to $c/(2B)$, which agrees with the general formula (1).

It is important to highlight that the aforementioned Fourier transform operation is digitally performed after the acquisition of the low-pass-filtered beat signal. If $R_{\max}$ is the maximum range of targets from which echoes are processed, then the maximum frequency of the beat signal becomes

$$f_{b,\max} = \frac{2\gamma R_{\max}}{c}. \tag{7}$$

For short-range applications, such as the tracking of vital signs, the above equation reveals that the bandwidth of the beat signal is usually much lower than the transmitted one B. This alleviates the sampling-speed requirements for the ADC in the deramping-based architecture of Fig. 3, and inexpensively enables these short-range LFMCW radars to be produced as commercial off-the-shelf (COTS) items [34]–[36].

A. Coherence Issues

An incoherent radar can only obtain range profiles. A coherent radar also preserves phase information, and consequently, can extract Doppler signatures. The phase maintaining is a key issue for the current application so that a careful design of the radar becomes mandatory to guarantee coherence.

For an LFMCW radar intended to monitor vital signs, a close look must be given at the exponential factor in (6). The desired phase history $\phi_d(\tau)$ is simply related to the range evolution of the target $R(\tau)$ by

$$\phi_d(\tau) = \frac{4\pi f_c R(\tau)}{c}. \tag{8}$$

Hence, a proper slow-time range tracking of the target requires the preservation of the phase history $\phi_d(\tau)$. This necessary phase control must be obtained not only in the waveform generation, but also in the acquisition process. In relation to the former, Fig. 4 depicts the waveform in the time domain.

The initial phase, highlighted by arrows in this figure, must be equal—or, at least, known—for each signal period. This is normally not a problem, as it can be assured by using available direct digital synthesis (DDS) and voltage-controlled oscillator (VCO) technologies. The irrelevant unprocessed interval T_u indicated in Fig. 4 might be useful to guarantee this phase match between transmitted ramps.[3] More importantly, in relation to the latter, the generation and acquisition processes must share a common clock, or at least, the clock shifts must be known. In other words, the samples taken by the ADC must be synchronized with the produced ramps in order to guarantee that no additional unknown phase term is added to (8). For example, if this undesired additional term turns out to be a white uniform stochastic process between $-\pi$ and π, then the wanted phase (8) is destroyed and the desired range evolution of the target cannot be recovered.

B. Extraction of Range History

In the following, by assuming that coherence is properly preserved, an algorithm to precisely extract the phase-based range evolution of a point scatterer is described. Basically, the algorithm adapts the data to finally extract the phase contained in the exponential factor of (6). From this unwrapped phase, obtaining the range evolution becomes trivial after (8).

Assume that the beat-signal samples associated with distinct ramp intervals are stacked in rows. This constitutes the raw-data matrix in fast- and slow-time dimensions, which is denominated $\mathbf{M}[n,m]$ ($n = 1,2,\ldots,N$; $m = 1,2,\ldots,M$, N being the number of transmitted ramps and M being the number of samples per ramp). The corresponding signal processing to derive the range evolution $R(\tau)$ of the target is divided into the following steps [24].

Step 1) Perform a fast Fourier transform (FFT) over each row of the raw-data matrix $\mathbf{M}[n,m]$. Denote this resulting range-profile matrix as $\mathbf{RP}[n,m]$.

Step 2) Choose the range bin m^* in which the target is found. Synthesize the signal $s[n] = \mathbf{RP}[n,m^*]$, which is a column of the matrix $\mathbf{RP}[n,m]$.

Step 3) Extract the phase of the signal $s[n]$ and unwrap it. Denote this phase as $\psi[n]$.

Step 4) Obtain the estimation of the scatterer range history as $\hat{R}[n] = c\psi[n]/(4\pi f_c)$.

In addition, four important issues must be highlighted before concluding this principle-of-operation section.

- The unwrapping process is necessary because the measured phase always takes values between $-\pi$ and π. This unwrapping will be successful if the phase jump between any two consecutive ramps is not greater than 2π. This means that the target range motion—along LOS—between any two consecutive periods must not exceed $0.5c/f_c$. This is usually met, as later verified by the provided simulated and live examples.[4]
- It is obvious that the target must remain in the same range bin during the entire coherent processing interval (CPI). Otherwise, it would not be possible to find a single column of matrix $\mathbf{RP}[n,m]$ in which the target situates. In the considered vital-sign monitoring scenario, range migrations are less likely to occur. Nevertheless, if these migrations arise, range-bin alignment algorithms with preservation of phase may be executed [37], [38].
- For the proposed method, it easily comes to light how clutter isolation is achieved. If the desired target is contained in the range bin m^*, other undesired targets—clutter—situated at other ranges will have little influence on the phase of the range bin m^*. As a consequence, a large-signal bandwidth is preferred to be transmitted in order to increase the range resolution.
- As the algorithm suggests, the extraction of the range is based on phase measurements, which usually implies a high precision. From (8), the range precision σ_R—this parameter must not be confused with the range resolution ΔR—can be written as $\sigma_R = \sigma_\phi c/(4\pi f_c)$, where σ_ϕ is the precision in the phase measurement. This means that higher precision is achieved for shorter wavelengths.

[3] If the generation block uses a phase-locked loop (PLL), this interval T_u can be useful to circumvent locking-related issues.

[4] Note that this bound is also $\lambda/2$, where $\lambda = c/f_c$ is the wavelength.

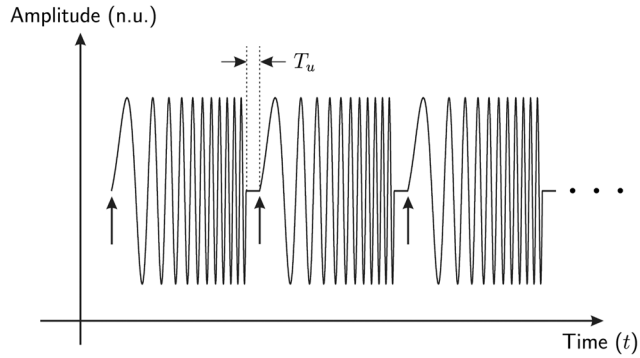

Fig. 4. Coherence maintenance: the initial phase of each transmitted ramp must be controlled.

TABLE I
RADAR PARAMETERS FOR SIMULATION

Parameter	Values
Center Frequency (f_c)	5.8 GHz
Instantaneous Transmitted Bandwidth (B)	160 MHz
Pulse Repetition Frequency (PRF)	200 Hz
Coherent Processing Interval (CPI)	12 s
Sampling Frequency (f_s)	8 KHz
Number of Samples per Ramp (M)	40
Number of Transmitted Ramps (N)	2400

III. SIMULATION RESULTS

In this section, simulations are carried out to verify the correct design of the range-tracking algorithm for a deramping-based LFMCW radar. The radar parameters for all the simulations presented here were selected as listed in Table I. Note that, in accordance with the vital-sign monitoring application, the required sampling frequency f_s is much lower than the transmitted bandwidth B. This results in the previously indicated alleviation in terms of sampling speed in the ADC for the deramping-based LFMCW radar architecture of Fig. 3.

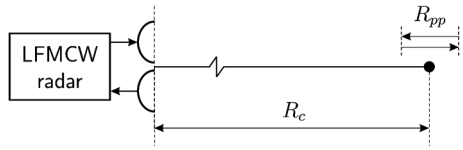

Fig. 5. Point scatterer sinusoidally vibrating along LOS.

TABLE II
MOTION PARAMETERS FOR THE POINT SCATTERER

Parameter	Values
Mean Range (R_c)	5.625 m
Peak-to-peak Sinusoidal Motion (R_{pp})	30 cm
Motion Frequency (f_t)	0.5 Hz

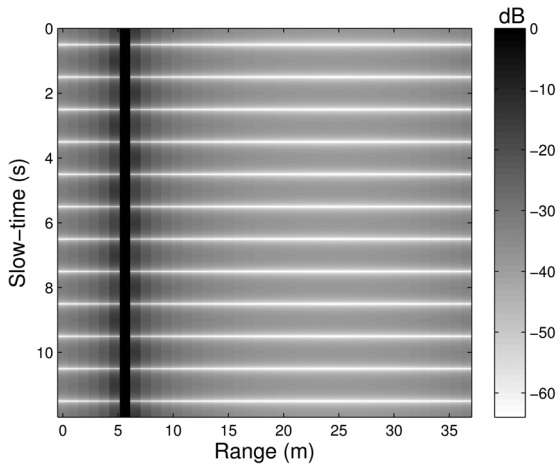

Fig. 6. Range profiles for the point-scatterer simulation.

A. Proof-of-Concept Simulation

Consider the LFMCW radar is illuminating a point scatterer, which is sinusoidally vibrating along the LOS. Fig. 5 depicts the corresponding scenario and Table II details the motion parameters of the target.

Fig. 6 shows the range-profile matrix $\mathbf{RP}[n, m]$ after applying a 40-point FFT to the acquired raw-data beat-signal matrix $\mathbf{M}[n, m]$. Note that the target appears at the seventh range bin and that no migration occurs since the range resolution ($\Delta R = 93.75$ cm) is greater than the target motion excursion ($R_{pp} = 30$ cm) and $R_c/\Delta R$ is exactly equal to 6. Nevertheless, if migration exists—for instance, because of an overall translational motion of the target—it can be easily corrected by means of advanced range-bin alignment techniques, which do not influence the phase history, such as the global range alignment or the extended envelope correlation procedures [37], [38].

The target phase must be extracted and unwrapped for this seventh range bin. Note that the maximum target LOS motion between two consecutive ramps is $\pi R_{pp} f_t/\mathrm{PRF} = 2.4$ mm, which is much lower than the aforementioned bound $0.5c/f_c = 25.9$ mm under which it is guaranteed that the phase unwrapping operation works correctly. This rule must be always checked, especially in the case of millimeter-wave radars for which the bound is reduced since the transmitted center frequency is considerably increased.

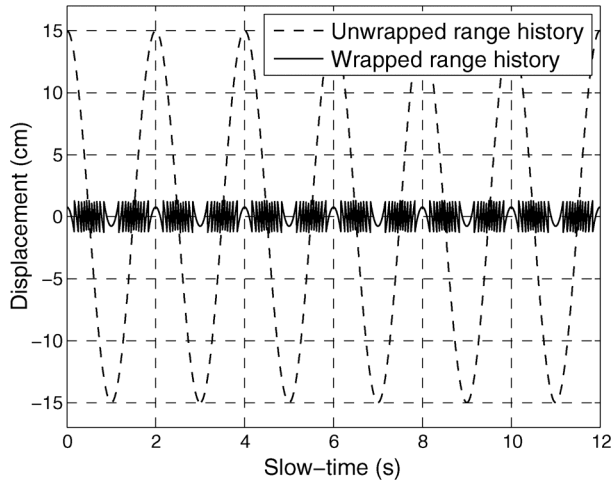

Fig. 7. Wrapped and unwrapped range history obtained for the sinusoidally vibrating point scatterer.

Fig. 7 details the wrapped and unwrapped range history of the target, after the trivial step $\hat{R}[n] = c\psi[n]/(4\pi f_c)$. The obtained range evolution for the target perfectly matches its 30-cm peak-to-peak sinusoidal motion. Hence, for a very high SNR, a very accurate tracking of the target can be achieved. This kind of result is very desirable for vital signs. Note that an absolute precise ranging of the target is not the objective here. In fact, for this example, as far as absolute ranges are concerned, the basic conclusion is that the target is at the seventh range bin ($R_c = 5.625$ m) so it is situated at some range between $[R_c - \Delta R/2]$ and $[R_c + \Delta R/2]$.[5] This is an important point to make because other radar prototypes, such as Doppler radars, do not have the capability to mark absolute ranges since they do not transmit an instantaneous bandwidth. Nevertheless, the important result for vital-sign applications is the one shown in Fig. 7. In this context, the obtaining of the target absolute range has no relevance.

B. Robustness Against Clutter

The proof-of-concept example of the previous section describes an ideal scenario with a point scatterer. A more realistic situation may include clutter, which has a greater influence on conventional Doppler radars than on the proposed LFMCW radar architecture. The reason for that must be found in the range-isolation capabilities of the proposed technique. To show it, consider the same simulation of Section III-A with the inclusion of an additional point scatterer uniformly moving along LOS from a range of 1 m to a range of 15 m during the CPI of 12 s. This implies that this clutter scatterer is moving away with a velocity of 1.17 m/s.

Fig. 8 shows the range-profile matrix for this simulation. As can be seen, the desired sinusoidally vibrating target is contained in the seventh range bin, whereas the clutter scatterer migrates through range cells. The two targets are at the same range bin at the slow-time instant 4 s approximately.

The range history extracted from the seventh range bin is shown in Fig. 9. Clutter has a strong influence on the correct

[5]To be rigorous, the absolute-range precision of a single target can be better than the range resolution if the SNR is high enough [28], [29].

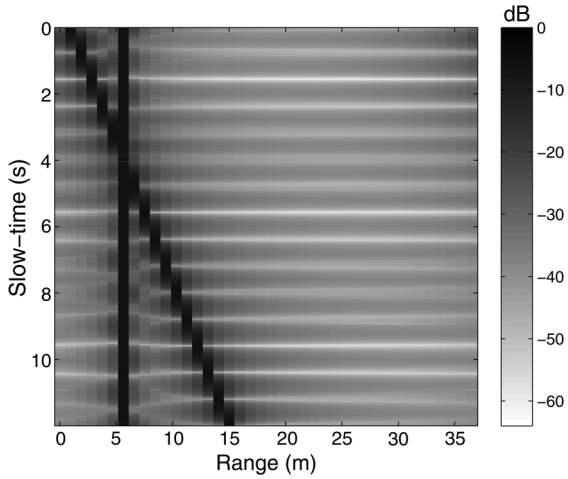

Fig. 8. Range profiles for the simulation with a desired scatterer and a clutter scatterer.

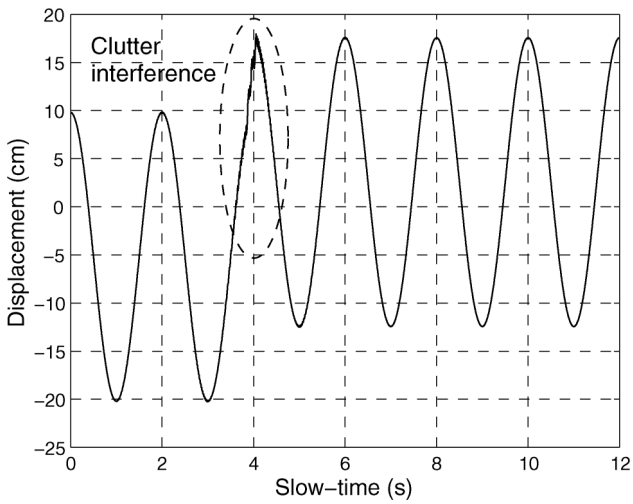

Fig. 9. Range history obtained for the desired target in the clutter scenario.

estimation of the desired range history during the time at which the two scatterers are at the same range bin. For other slow-time intervals, the interference is minor and then the desired range history can be properly tracked. The dc offset observed in Fig. 9 has its origin in the phase unwrapping process.

This example proves that LFMCW radars can take benefit from this range-isolation capability. Furthermore, it reveals the property of transmitting large bandwidths for increasing range resolution, and thus, improving the isolation features.

C. Robustness Against Noise

Noise is always present in RF systems. This noise, which mostly has a thermal origin, is normally modeled as additive, white, and Gaussian. Subsequently, its influence on the operation of the deramping-based LFMCW radar for this context is analyzed. Fig. 10 plots the mean square error (MSE) as a function of the SNR, after a Monte Carlo simulation with 1000 realizations for each graph point. Signal power is the power of the beat signal for the same example of Section III-A. The two graphs in Fig. 10 correspond to different target mean

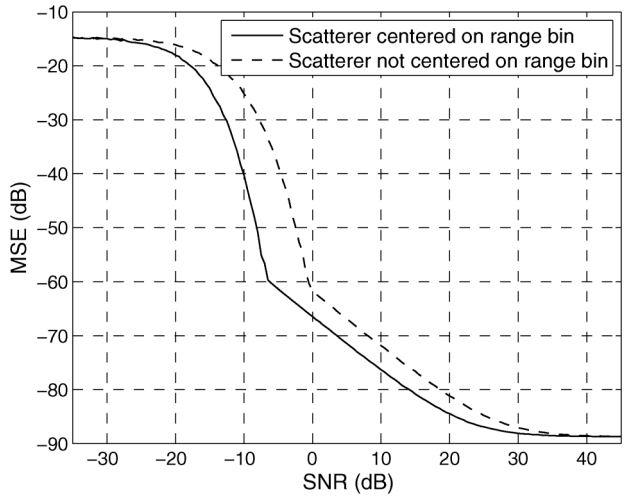

Fig. 10. Performance analysis against noise. The MSE is represented as a function of the SNR.

ranges; specifically, for a target centered on the range bin ($R_c = 5.625$ m) and for a target located at a range-bin extreme ($R_c = 5.15625$ m). If $R_t[n]$ is the desired real zero-mean range history of the target and $\hat{R}_t[n]$ is the algorithm estimate, the MSE is defined as

$$\mathrm{MSE} = \frac{1}{N}\sum_{n=1}^{N}\left(R_t[n] - \hat{R}_t[n]\right)^2. \tag{9}$$

A very low SNR obviously implies that the range history cannot be recovered. The maximum error for low SNRs saturates because the phase is wrapped in the interval $[-\pi, \pi]$. Note that a perfect reconstruction can be achieved for high SNRs—the MSE asymptotes to a minimum numerical simulation error. Besides, it can be seen that, for a given MSE, a lower SNR is necessary for the case in which the point scatterer is located at the center of the range bin. This is congruent with the fact that the energy from the target is transferred to other range bins when it is shifted from the middle of the range bin.

Finally, the 1-dB/1-dB slope observed in Fig. 10 when the SNR approximately ranges from 0 to 20 dB can be theoretically predicted, being the demonstration analogous to the analysis of analog communications systems in the presence of noise [39].

Fig. 11 shows the estimated and real range history of the target for an SNR of -15 dB. Even for such a low SNR, the periods of the target motion can be perfectly identified.

D. Multiple-Scatterer Simulation

A real vital-sign monitoring scenario—e.g., breathing tracking—is more complex than a single point scatterer moving forward and backward during the CPI. First of all, the hypothesis of a single point scatterer is no longer valid. Conversely, in the intended biomedical application, the chest can be considered to be shaped by multiple scatterers moving in phase, but with a different motion amplitude. Moreover, it must be assumed that the RCS of each scatterer is different and changes during the CPI; i.e., the so-called "target scintillation" always exists [28],

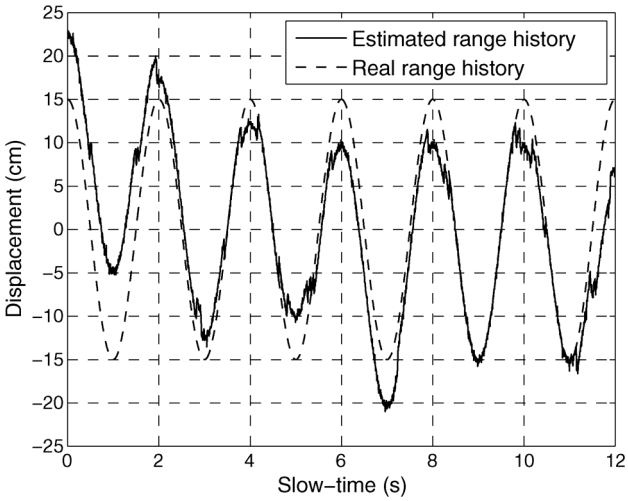

Fig. 11. Estimated and real range history for a sinusoidally vibrating scatterer with an SNR of −15 dB ($R_c = 5.625$ m).

TABLE III
MOTION PARAMETERS FOR A MULTIPLE-SCATTERER TARGET

Parameter	Values
Number of Scatterers (K)	100
Mean Range (R_c)	5.625 m
Maximum Peak-to-peak Sinusoidal Motion ($R_{pp,\max}$)	1 cm
Motion Frequency (f_t)	0.5 Hz
Maximum Target RCS ($RCS_{\max}$)	1 m^2

[29]. Table III details the parameters for a simulation scenario with multiple in-phase moving scatterers.

In this simulation, the peak-to-peak range motion for each scatterer is independently drawn from a uniform distribution in the interval $[0, R_{pp,\max}]$. By analogy, the RCS for each scatterer and for each ramp is independently obtained from a uniform distribution in the interval $[0, \mathrm{RCS}_{\max}]$. The estimated range history for this multiple-scatterer case is shown in Fig. 12. For comparison, the ideal range history for the maximum motion $R_{pp,\max}$ is also depicted in Fig. 12. As can be seen, the periods of the in-phase moving scatterers are clearly shown and no interference between them is observed, which is in contrast to the results of Section III-B. This is encouraging because the vital-sign cycles are normally required to be obtained, whereas the maximum amplitude is usually unimportant. Very little noise due to the target scintillation phenomenon appears in the extracted phase-based range track.

The validity of these simulations is confirmed in the next section, where a description of a developed LFMCW radar prototype and measurement results of live experiments are presented. Note that the use of an LFMCW radar does not circumvent other important limiting issues arising when dealing with vital signs, such as the so-called "random body movement" (RBM) [40], which remains as further research work to be addressed. An additional interesting issue is the obvious necessity of directive antennas to better concentrate the radiation. This suggests the exploitation of high frequencies—e.g., millimeter-wave frequencies—for future radar prototypes.

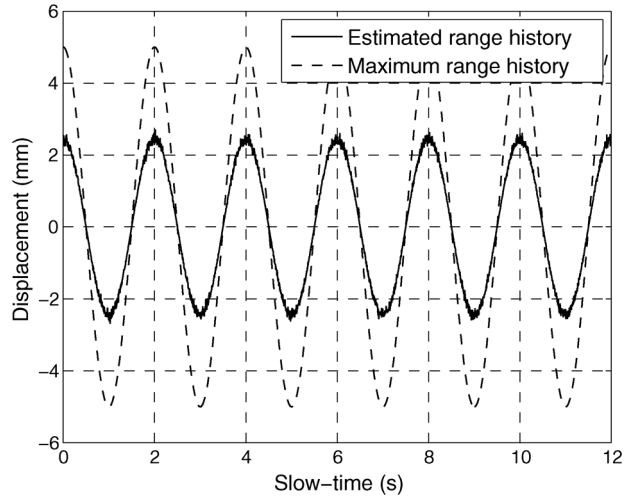

Fig. 12. Range histories for the multiple-scatterer simulation.

IV. LFMCW RADAR SYSTEM PROTOTYPE AND EXPERIMENTAL RESULTS

This section presents the development of a proof-of-concept coherent LFMCW radar sensor prototype. The built radar system is also evaluated through four different experiments with emphasis on small displacement tracking. These tests are configured to confirm its capability in terms of absolute range detection, tracking of distinct motion patterns, and real vital-sign sensing.

A. Description of the LFMCW Radar System Prototype

The block diagram of the implemented coherent LFMCW radar system—Tx, Rx, and signal-acquisition modules—is shown in Fig. 13. Its main parts are described as follows.

- In the Tx chain, the National Instruments PXIe 1075 chassis integrating three functional blocks is used.[6] Following the signal-generation sequence, these building blocks are: 1) the PXIe 5450 (programmable baseband vector signal generator that can precisely define both the frequency and phase, and thus, make possible the coherent LFMCW signal creation), 2) the PXIe 5611 and PXIe 5652 (up-converter driven by the local oscillator), and 3) the PXIe 5691 (variable RF gain block). The final output of the PXIe 1075 chassis is an RF LFMCW chirp signal that sweeps its instantaneous frequency from 5.72 to 5.88 GHz (i.e., 160-MHz bandwidth centered at 5.8 GHz) within a duration time of 2 ms (i.e., PRF of 500 Hz). A Wilkinson-type power divider is employed to split the chirp signal into two components. One of them serves as the local oscillator of the mixer to down-convert the received signal in the practical realization of the deramping process, whereas the other one is fed into a power amplifier with a 30-dB gain level to compensate propagation attenuation and absorption loss effects.
- In the RX part, two low-noise amplifiers followed by a gain block amplify the weak received signal with a total gain of 47.5 dB. The last stage of the RF end is a quadrature

[6][Online]. Available: http://sine.ni.com/nips/cds/print/p/lang/es/nid/205962

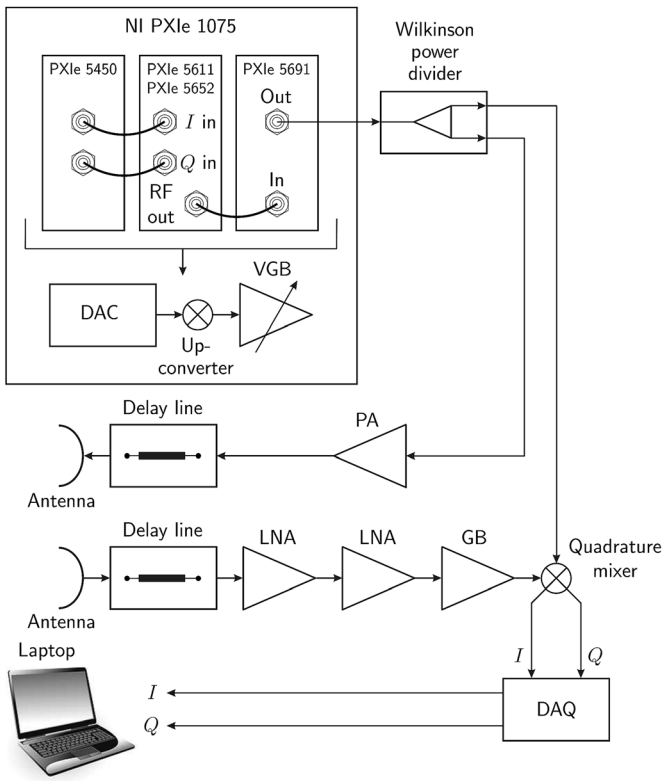

Fig. 13. Block diagram of the developed LFMCW radar system prototype (power amplifier: PA; low-noise amplifier: LNA; digital-to-analog converter: DAC; data acquisition: DAQ; gain block: GB; and variable gain block: VGB).

down-converter where the received signal is mixed with the transmitted one so that the I/Q output—i.e., the beat signal—is digitized with a 10-kHz-sampling-rate data acquisition block for signal processing.

- As radiating elements, two independent antennas for the Tx and Rx consisting of 2×2 planar patch arrays are employed. As explained in Section II, this was done to further increase the isolation between the transmitted and received signals, which can seriously degrade the radar performance. Moreover, the directivity enhancement attained through the array solution in relation to a single patch enables to better focus on the desired target and to more efficiently reject the nearby clutter, which can lead to interference for both displacement tracking and absolute range detection.

In addition, a delay line is inserted between the antenna and the amplifier at both the Tx and Rx sides to physically extend the delay time. This was done to keep the desired beat frequency away from the low-frequency noisy zone and guarantee a robust performance. Indeed, for indoor-detection applications, the targets are usually very close to the radar. Therefore, the small time delay appearing between transmitted and received signals produces a very small frequency difference (beat frequency) between the local oscillator and RF ports of the down-converter. Delay lines can then help to avoid the flicker noise—i.e., the $1/f$ noise—of the mixer by shifting the beat frequency to a higher range. This is very desirable, taking into account that the low-frequency spectrum is often not clean also due to other effects, such as the direct antenna coupling from the Tx to the Rx module. On the other hand, given the limited operating bandwidth of the developed radar system, it is obvious that the group velocity difference in the delay line can be safely neglected. This means that the extra time delay introduced by the delay line is constant. Hence, a simple calibration can easily eliminate the inherent time delay within the circuit. Moreover, since the extra time delay comes from the radar hardware and is assumed to be constant during the experiments, a one-time calibration is enough as long as the circuit setup remains the same.

A photograph of the constructed LFMCW radar system is depicted in Fig. 14. Subsequently, to extensively corroborate the theoretical and simulation results presented in Sections II and III and demonstrate practical viability, the developed prototype of the LFMCW radar sensor has been tested in various scenarios. Specifically, four different experiments were carried out attending to the measurement setups shown in Fig. 15. The first experiment in Fig. 15(a), detailed in Section IV-B, aims to evaluate the absolute range detection capability of the proposed radar system. Note that range-information detection is the basic function of LFMCW radars and their main advantage over other remote-sensing systems, such as Doppler radars, which can only track small displacements and have been widely used in wireless vital-sign detection applications. The next two experiments, shown in Fig. 15(b) and (c) and described in Section IV-C, are carried out to prove that the implemented radar system can accurately track several motion patterns. To conclude, Section IV-D investigates the performance of the radar prototype in a real vital-sign sensing scenario in order to verify its feasibility in biomedical/heathcare environments, as shown in Fig. 15(d).

B. Absolute Range Detection and Performance Evaluation

In the first experiment, a metal plate acting as a target was placed on a small cart so that it could move along a ruler with certain step size [see Fig. 15(a)]. Due to the internal hardware delay, a calibration of the radar system was necessary before initiating the range-detection test. Such calibration was performed when the target was 4.5 ft (137.16 cm) away from the radar. For this experiment, the target moved along the ruler from a distance to the radar of 3 ft (91.44 cm) to 12 ft (365.76 cm) with a step size equal to 6 in (15.24 cm). The detected reference beat frequency during the calibration process is shown in Fig. 16(a). Here, the x-axis value of the normalized-amplitude peak corresponds to the beat frequency. According to (5), the change in the beat frequency is linearly proportional to the variation of the distance. The values of the detected beat frequencies and the corresponding ranges at different locations along the ruler are provided in Table IV. The standard error listed in the fourth row is the difference between the detected range and the reference distance measured by the ruler. As observed and in agreement with the discussion in Section III-A, the maximum error is less than 0.5 ft (15.24 cm) and the relative error is below 5%. This error mostly came from the limited beat frequency resolution of the radar system, which is proportional to its operating bandwidth, as stated in (1). It should also be appreciated that the range error was larger when the target was further away from radar. This is a logical result, taking into account the decrease in the reflected signal strength from the target—i.e., energy of the re-

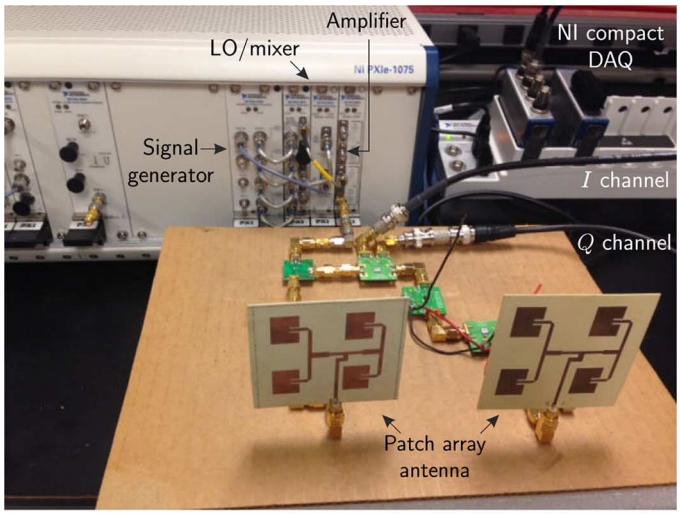

(a)

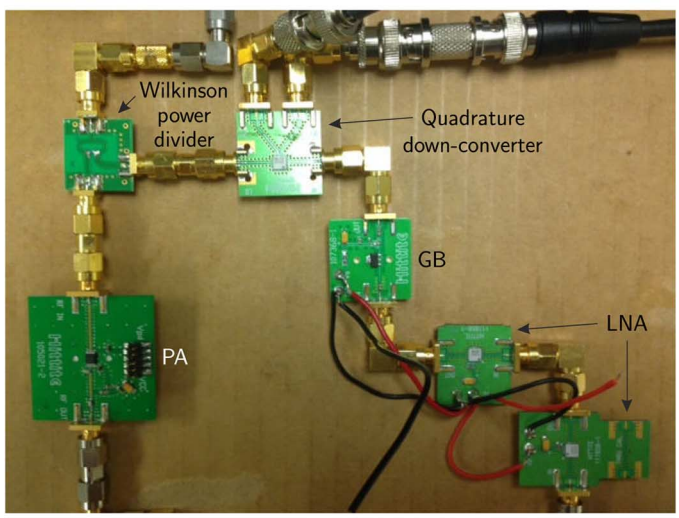

(b)

Fig. 14. Photograph of the developed LFMCW radar system prototype (power amplifier: PA; low-noise amplifier: LNA; data acquisition: DAQ; gain block: GB; and local oscillator: LO). (a) Complete view. (b) Detail.

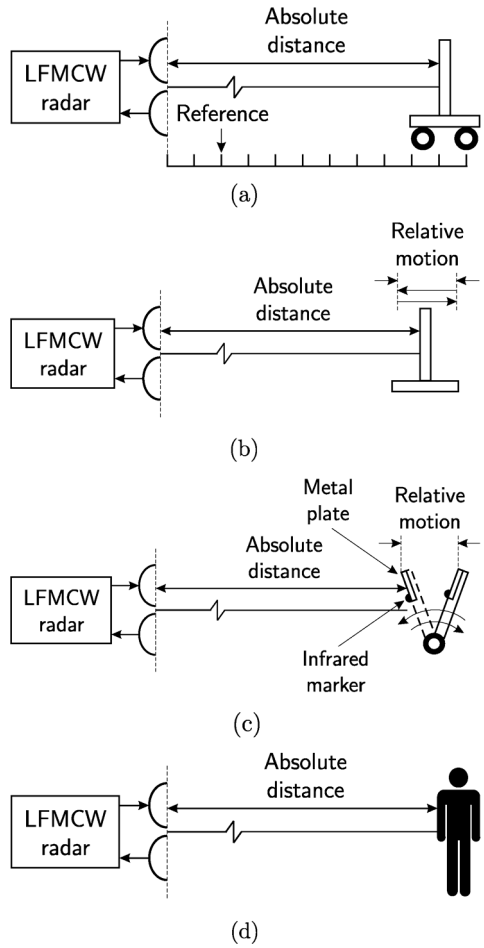

Fig. 15. Experimental setups. (a) Range-detection test. (b) Sinusoidal-motion tracking test. (c) Motion-tracking test with stop periods. (d) Human vital-sign sensing test.

ceived echo—with the distance. As a proof of that, as Fig. 16(b) attests for the target located at 8.5 ft (259.08 cm), note that the peak level due to the target reflection is weaker than that associated with the Tx-to-Rx coupling effect and comparable to the peaks caused by the surrounding clutter. This makes the obtained results more vulnerable to the interference phenomenon than to such imperfection in the radar hardware.

C. Displacement Measurement Accuracy

An extensive theoretical and simulation study about the displacement tracking performance of the deramping-based LFMCW radar approach was described in the previous sections. The second and third tests were aimed at experimentally validating this capability in the developed radar prototype.

First, as real implementation of the scenario of Fig. 5, an actuator was used to generate a sinusoidal motion in the metal plate with a peak-to-peak amplitude of 1.5 cm and a period of 4.762 s [see Fig. 15(b)]. The initial distance between the radar antenna and the target was set to be 1 m. Fig. 17 shows the detected displacement and a comparison with the ground truth motion of the actuator. As can be seen, a fairly close agreement between both motion patterns was obtained with an error less than 1 mm.

It is worth mentioning that a sinusoidal motion does not possess dc information. However, a real respiration is a motion that contains a short stationary period after the lung deflation. For an all-round health care, there is a practical need for the radar sensor to be able to accurately measure the respiration pattern, which has both ac and dc information. Therefore, in order to also consider the above relevant aspect in a more realistic environment, a professional phantom widely used to mimic the chest movement in hospitals was utilized to serve as the target in a subsequent experiment [see Fig. 15(c)]. To qualify the obtained performance in this situation, Fig. 18 represents the measured displacement curve and its comparison with the reference. This reference displacement was obtained through a real-time position management (RPM) system from Varian Medical Systems, Palo Alto, CA, USA.[7] The RPM system is a respiration monitoring approach widely used in clinical radiotherapy so as to

[7][Online]. Available: http://www.varian.com/us/oncology/radiation_oncology/clinac/rpm_respiratory_gating.html

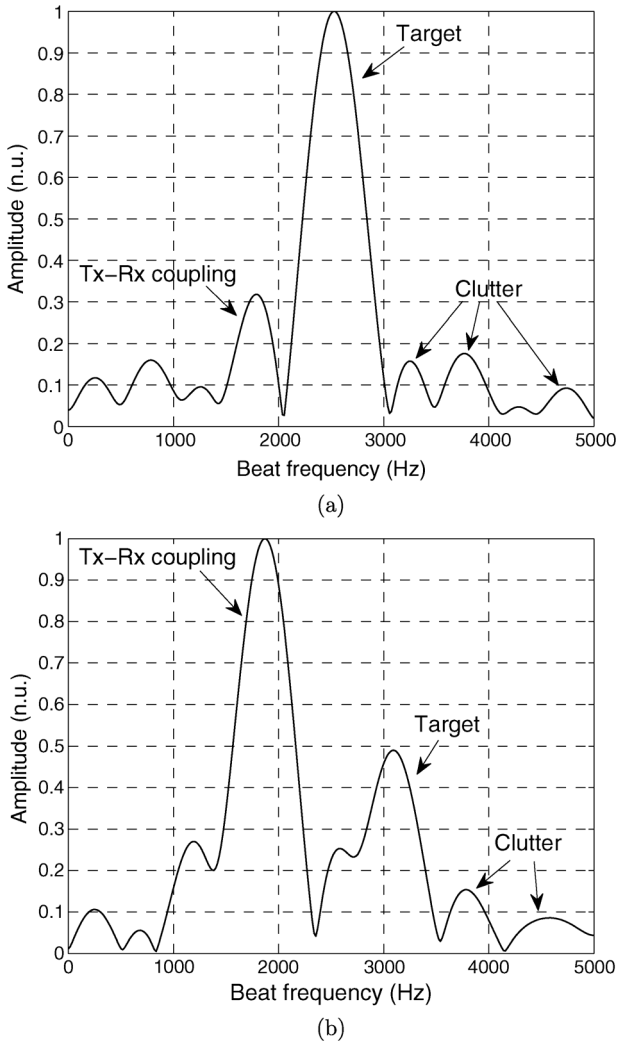

Fig. 16. Normalized-amplitude representation of the measured beat frequency for different target locations. (a) Target located at 4.5 ft (137.16 cm)—calibration distance. (b) Target located at 8.5 ft (259.08 cm).

TABLE IV
EXPERIMENTAL PERFORMANCE OF ABSOLUTE DISTANCE DETECTION

Parameter Values			
Reference Distance (ft/cm)	Beat Frequency (Hz)	Measured Distance (ft/cm)	Standard Error (ft/cm)
3.0/91.44	2305.8	3.11/94.79	$+0.11/+3.35$
3.5/106.68	2401.1	3.69/112.47	$+0.19/+5.79$
4.0/121.92	2456.1	4.03/122.83	$+0.03/+0.91$
4.5/137.16	2531.3	4.50/137.16	0.00/0.00
5.0/152.40	2606.5	4.96/151.18	$-0.04/-1.22$
5.5/167.64	2656.6	5.27/160.63	$-0.23/-7.01$
6.0/182.88	2731.8	5.73/174.65	$-0.27/-8.23$
6.5/198.12	2807.0	6.19/188.67	$-0.31/-9.45$
7.0/213.36	2882.2	6.66/203.00	$-0.44/-13.41$
7.5/228.60	2957.6	7.12/217.02	$-0.43/-13.11$
8.0/243.84	3022.4	7.52/229.21	$-0.48/-14.63$
8.5/259.08	3105.3	8.03/244.75	$-0.47/-14.32$
9.0/274.32	3222.2	8.75/266.70	$-0.25/-7.62$
9.5/289.56	3272.0	9.16/279.20	$-0.34/-10.36$
10.0/304.80	3339.1	9.57/291.69	$-0.43/-13.11$
10.5/320.40	3406.0	10.08/307.24	$-0.42/-12.80$
11.0/335.28	3523.0	10.60/323.09	$-0.40/-12.19$
11.5/350.52	3606.0	11.11/338.63	$-0.39/-11.89$
12.0/365.76	3673.0	11.62/354.18	$-0.38/-11.58$

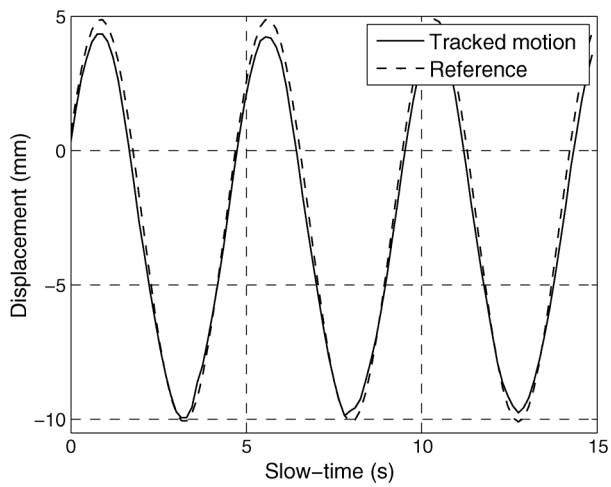

Fig. 17. Detected motion pattern of the moving plate and comparison with the reference pattern.

be very accurate. It employs an infrared camera to track the infrared marker on the phantom.

Regarding Fig. 18, note that the detected amplitude is slightly larger than the reference one. The reason for that must be found in the two different tracking approaches; for the infrared camera, the marker can be understood as a single point scatterer; for the proposed radar system, the reflected signal comes from the entire target surface. Thus, the radar measures the average motion of the metal plate. Fig. 15(c) shows that the phantom motion is driven by a motor, being the displacement of each scatterer of the metal plate surface slightly different. Indeed, the metal plate was attached to the end of the phantom and had a radius larger than the infrared marker. This justifies the differences observed in the two range histories. Nevertheless, the excellent match observed in Fig. 18 between the detected displacement from the proposed radar system prototype and the reference demonstrates that this radar sensor can accurately track the tiny displacement of various types of movement.

Thus far, it has been proven that the devised technique not only reveals the frequency of the periodical movement, but can also track the movement pattern with a very high precision. When compared to the dc coupled Doppler radar alternative reported in [11], this procedure is free from dc offset problems and does not require tedious dc voltage bias tuning.

D. Vital-Sign Sensing from Human Target

Finally, the experiment was moved on to a real human vital-sign sensing scenario [see Fig. 15(d)]. A photograph of the experiment setup arranged for this fourth test is depicted in Fig. 19.

Note that, unlike the metal plate, each point on the thoracic cavity wall has an inhomogeneous motion and distribution. Hence, different parts of the body or the surroundings have different ranges, which ultimately results in a small difference in the beat frequency. According to (6), such phenomenon makes the phase information in baseband no longer a linear summation of the phase information from each point. Therefore, for real human vital-sign sensing, the measurement result is expected to

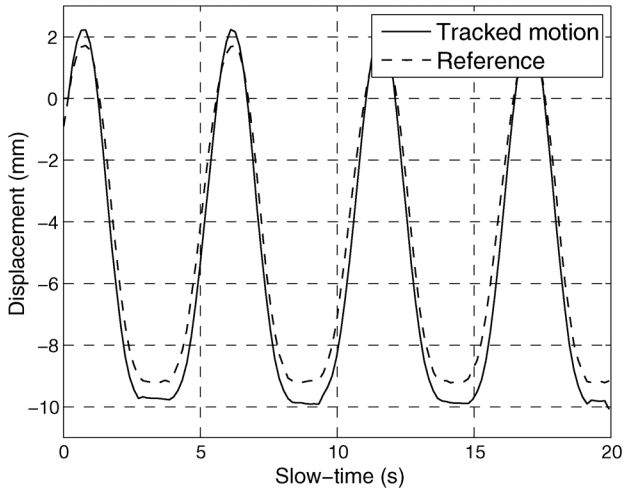

Fig. 18. Detected motion pattern of the phantom and comparison with the reference pattern.

Fig. 19. Photograph of the real experimental setup of the human vital-sign tracking test.

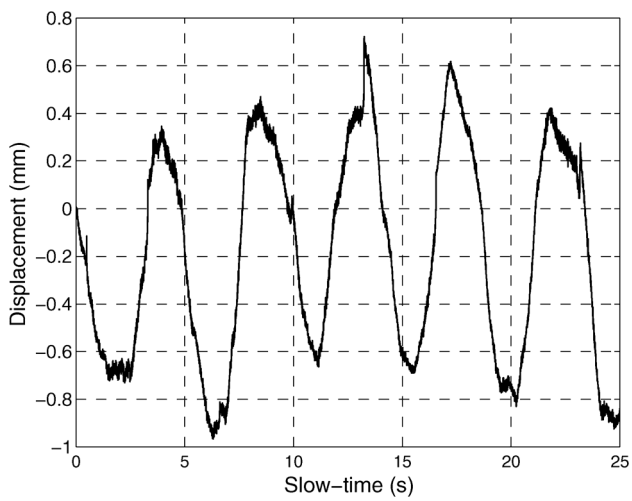

Fig. 20. Detected human respiration pattern.

be slightly distorted by the nearby clutter. Fig. 20 plots the measured human respiration detection result (normal breathing). The spike appearing at around the 13th second is attributable to the surrounding clutter, similar to the simulation results reported in Fig. 9. Furthermore, as discussed in Section III-D, the existence of multiple scatterers shrinks the amplitude of the tracked displacement. From both simulation and experiments, it has been found that this amplitude shrinkage is also related to static clutter in the proximity of the desired target. Note that, when the human subject is breathing, most parts of the body—i.e., clutter—other than the thoracic cavity do not heave. Hence, reflections from large stationary areas of the human subject interfere with reflections from the moving scatterers and thus cause the wanted signals to be smaller than predicted. Nevertheless, despite these distortions and amplitude shrinkage effects, the respiration pattern can still be clearly recognized.

V. Conclusions

Monitoring of vital signs without contact is an emerging and interesting application for short-range radars. In this paper, a deramping-based LFMCW radar scheme has been proposed. On one hand, this solution transmits instantaneous bandwidth; hence, minimizing the undesired effects of surrounding clutter in contrast to conventional Doppler radars. On the other hand, the algorithm to obtain the target range history is based on phase measurements; thus, improving range precision when compared to IR-UWB radar alternatives. Furthermore, the described LFMCW radar architecture is conceptually simple and the deramping process greatly simplifies its hardware implementation mainly in terms of sampling speed for the Rx ADC. A detailed theoretical analysis of the operating principle of this radar has been described with an emphasis on relevant issues for the addressed biomedical scenario such as coherence. Simulation results have been provided to validate this radar scheme and its phase-based range-tracking algorithm. Robustness against clutter, noise, and the presence of multiple scatterers has also been analyzed. Besides, an LFMCW radar prototype has been developed and real experiments corresponding to a metal plate and breathing subjects have been shown. Ongoing research work is the development and usage of millimeter-wave radar systems to better illuminate and isolate the desired target in this healthcare context.

Acknowledgment

The authors would like to acknowledge National Instruments for support on PXI microwave measurement and AWR Design Environment.

References

[1] C. Li, V. M. Lubecke, O. Boric-Lubecke, and J. Lin, "A review on recent advances in Doppler radar sensors for noncontact healthcare monitoring," *IEEE Trans. Microw. Theory Techn.*, vol. 61, no. 5, pp. 2046–2060, May 2013.

[2] B. Schleicher, I. Nasr, A. Trasser, and H. Schumacher, "IR-UWB radar demonstrator for ultra-fine movement detection and vital-sign monitoring," *IEEE Trans. Microw. Theory Techn.*, vol. 61, no. 5, pp. 2076–2085, May 2013.

[3] V. C. Chen and H. Ling, *Time-frequency Transforms for Radar Imaging and Signal Analysis*. Norwood, MA, USA: Artech House, 2002.

[4] V. C. Chen, *The Micro-Doppler Effect in Radar*. Norwood, MA, USA: Artech House, 2011.

[5] R. G. Raj, V. C. Chen, and R. Lipps, "Analysis of radar human gait signatures," *IET Signal Process.*, vol. 4, no. 3, pp. 234–244, Jun. 2010.

[6] A. F. García-Fernández, O. A. Yeste-Ojeada, and J. Grajal, "Facet model of moving targets for ISAR imaging and radar back-scattering simulation," *IEEE Trans. Aerosp. Electron. Syst.*, vol. 46, no. 3, pp. 1455–1467, Jul. 2010.
[7] J. M. Muñoz-Ferreras, F. Pérez-Martínez, and M. Burgos-García, "Helicopter classification with a high resolution LFMCW radar," *IEEE Trans. Aerosp. Electron. Syst.*, vol. 45, no. 4, pp. 1373–1384, Oct. 2009.
[8] N. Hafner, I. Mostafanezhad, V. M. Lubecke, O. Boric-Lubecke, and A. Host-Madsen, "Non-contact cardiopulmonary sensing with a baby monitor," in *Proc. 29th Annu. Int. IEEE Eng. Med. Biol. Soc. Conf.*, Lyon, France, Aug. 2007, pp. 2300–2302.
[9] C. Li, J. Lin, and Y. Xiao, "Robust overnight monitoring of human vital signs by a non-contact respiration and heartbeat detector," in *Proc. 28th Annu. Int. IEEE Eng. Med. Biol. Society Conf.*, New York, NY, USA, Aug. 2006, pp. 2235–2238.
[10] W. Massagram, N. Hafner, V. Lubecke, and O. Boric-Lubecke, "Tidal volume measurement through non-contact Doppler radar with DC reconstruction," *IEEE Sensors J.*, vol. 13, no. 9, pp. 3397–3404, Sep. 2013.
[11] C. Gu, R. Li, H. Zhang, A. Y. C. Fung, C. Torres, S. B. Jiang, and C. Li, "Accurate respiration measurement using DC-coupled continuous-wave radar sensor for motion-adaptive cancer radiotherapy," *IEEE Trans. Biomed. Eng.*, vol. 59, no. 11, pp. 3117–3123, Nov. 2012.
[12] C. Li, X. Yu, C. M. Lee, D. Li, L. Ran, and J. Lin, "High-sensitivity software-configurable 5.8-GHz radar sensor receiver chip in 0.13-μm CMOS for noncontact vital sign detection," *IEEE Trans. Microw. Theory Techn.*, vol. 58, no. 5, pp. 1410–1419, May 2010.
[13] J. C. Lin, "Noninvasive microwave measurement of respiration," *Proc. IEEE*, vol. 63, no. 10, p. 1530, Oct. 1975.
[14] A. D. Droitcour, O. Boric-Lubecke, V. M. Lubecke, and J. Lin, "0.25 μm CMOS and BiCMOS single-chip direct-conversion Doppler radars for remote sensing of vital signs," in *Proc. IEEE Int. Solid-State Circuits Conf.*, San Francisco, CA, USA, Feb. 2002, vol. 1, pp. 348–349.
[15] B. K. Park, V. M. Lubecke, and O. Boric-Lubecke, "Arctangent demodulation with DC offset compensation in quadrature Doppler radar receiver systems," *IEEE Trans. Microw. Theory Techn.*, vol. 55, no. 5, pp. 1073–1079, May 2007.
[16] A. Wiesner, "A multifrequency interferometric CW radar for vital signs detection," in *Proc. IEEE Radar Conf.*, Pasadena, CA, USA, May 2009, pp. 1–4.
[17] D. T. Petkie, C. Benton, and E. Bryan, "Millimeter wave radar for remote measurement of vital signs," in *Proc. IEEE Radar Conf.*, Pasadena, CA, USA, May 2009, pp. 1–3.
[18] H. R. Chuang, H. C. Kuo, F. L. Lin, T. H. Huang, C. S. Kuo, and Y. W. Ou, "60-GHz millimeter-wave life detection system (MLDS) for noncontact human vital-signal monitoring," *IEEE Sensors J.*, vol. 12, no. 3, pp. 602–609, Mar. 2012.
[19] T. E. McEwan, "Body monitoring and imaging apparatus and method," US Patent 5573012, Nov. 12, 1996.
[20] M. Y. W. Chia, S. W. Leong, C. K. Sim, and K. M. Chan, "Through-wall UWB radar operating within FCC's mask for sensing heart beat and breathing rate," in *Proc. Eur. Radar Conf.*, Paris, France, Oct. 2005, pp. 267–270.
[21] J. C. Y. Lai, Y. Xu, E. Gunawan, E. C. Chua, A. Maskooki, Y. L. Guan, K. S. Low, C. B. Soh, and C. L. Poh, "Wireless sensing of human respiratory parameters by low-power ultrawideband impulse radio radar," *IEEE Trans. Instrum. Meas.*, vol. 60, no. 3, pp. 928–938, Mar. 2011.
[22] Y. Nijsure, W. P. Tay, E. Gunawan, F. Wen, Z. Yang, Y. L. Guan, and A. P. Chua, "An impulse radio ultrawideband system for contactless noninvasive respiratory monitoring," *IEEE Trans. Biomed. Eng.*, vol. 60, no. 6, pp. 1509–1517, Jun. 2013.
[23] A. Nezirovic, S. Tesfay, A. S. E. Valavan, and A. Yarovoy, "Experimental study on human breathing cross section using UWB impulse radar," in *Proc. Eur. Radar Conf.*, Amsterdam, The Netherlands, Oct. 2008, pp. 1–4.
[24] G. Wang, J. M. Muñoz-Ferreras, C. Gu, C. Li, and R. Gómez-García, "Linear-frequency-modulated continuous-wave radar for vital-sign monitoring," in *Proc. IEEE Biomed. Wireless Technol., Networks, Sens. Syst. Top. Conf.*, Newport Beach, CA, USA, Jan. 2014, pp. 1–3.
[25] F. K. Wang, T. S. Horng, K. C. Peng, J. K. Jau, J. Y. Li, and C. C. Chen, "Detection of concealed individuals based on their vital signs by using a see-through-wall imaging system with a self-injection-locked radar," *IEEE Trans. Microw. Theory Techn.*, vol. 61, no. 1, pp. 696–704, Jan. 2013.
[26] G. Wang, C. Gu, T. Inoue, and C. Li, "Hybrid FMCW-interferometry radar system in the 5.8 GHz ISM band for indoor precise position and motion detection," in *Proc. IEEE MTT-S Int. Microw. Symp.*, Seattle, WA, USA, Jun. 2013, pp. 1–3.
[27] P. D. Fisher, "Improving on police radar," *IEEE Spectr.*, vol. 29, no. 7, pp. 38–43, Jul. 1992.
[28] M. I. Skolnik, *Introduction to Radar Systems*, 3rd ed. New York, NY, USA: McGraw-Hill, 2002.
[29] M. A. Richards, J. A. Scheer, and W. A. Holm, *Principles of Modern Radar. Basic Principles*, 2nd ed. Edison, NJ, USA: SciTech, 2010.
[30] J. M. Muñoz-Ferreras and R. Gómez-García, "A deramping-based multiband radar sensor concept with enhanced ISAR capabilities," *IEEE Sensors J.*, vol. 13, no. 9, pp. 3361–3368, Sep. 2013.
[31] W. G. Carrara, R. S. Goodman, and R. M. Majewski, *Spotlight Synthetic Aperture Radar: Signal Processing Algorithms*. Boston, MA, USA: Artech House, 1995.
[32] D. R. Wehner, *High-Resolution Radar*, 2nd ed. Boston, MA, USA: Artech House, 1995.
[33] W. J. Caputi, "Stretch: A time transformation technique," *IEEE Trans. Aerosp. Electron. Syst.*, vol. AES-7, no. 2, pp. 269–278, Mar. 1971.
[34] E. C. Zaugg, D. L. Hudson, and D. G. Long, "The BYU μSAR: A small, student-built SAR for UAV operation," in *Proc. Int. Geosci. Remote Sens. Symp.*, Denver, CO, USA, Aug. 2006, pp. 411–414.
[35] M. Edrich, "Design overview and flight test results of the miniaturised SAR sensor MISAR," in *Proc. 1st Eur. Radar Conf.*, Amsterdam, The Netherlands, Oct. 2004, pp. 205–208.
[36] P. Almorox-Gonzalez, J. T. González-Partida, M. Burgos-García, C. de la Morena-Álvarez-Palencia, L. Arche-Andradas, and B. P. Dorta-Naranjo, "Portable high resolution LFM-CW radar sensor in millimeter-wave band," in *Proc. Int. Sensor Technol. Appl. Conf.*, Valencia, Spain, Oct. 2007, pp. 5–9.
[37] J. Wang and D. Kaslingam, "Global range alignment for ISAR," *IEEE Trans. Aerosp. Electron. Syst.*, vol. 39, no. 1, pp. 351–357, Jan. 2003.
[38] J. M. Muñoz-Ferreras and F. Pérez-Martínez, "Subinteger range-bin alignment method for ISAR imaging of noncooperative targets," *EURASIP J. Adv. Signal Process.*, vol. 2010, no. 1, pp. 1–16, Jan. 2010.
[39] J. G. Proakis and M. Salehi, *Communications Systems Engineering*, 2nd ed. Upper Saddle River, NJ, USA: Prentice-Hall, 2002.
[40] C. Li and J. Lin, "Random body movement cancellation in Doppler radar vital sign detection," *IEEE Trans. Microw. Theory Techn.*, vol. 56, no. 12, pp. 3143–3152, Dec. 2008.

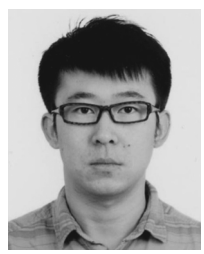

Guochao Wang (S'11) received the B.S. and M.S. degrees in electronics and information engineering from Northwestern Polytechnical University, Xi'an, Shaanxi, China, in 2007 and 2010, respectively, and is currently working toward the Ph.D. degree in electrical engineering with Texas Tech University, Lubbock, TX, USA.

He is currently with the Department of Electrical and Computer Engineering, Texas Tech University. His research interests include microwave/RF wireless sensors and microwave/millimeter-wave circuit and system design.

José-María Muñoz-Ferreras received the Telecommunication Engineer and Ph.D. degrees in electrical and electronic engineering from the Polytechnic University of Madrid, Madrid, Spain, in 2004 and 2008, respectively.

He is currently with the Department of Signal Theory and Communications, University of Alcalá, Alcalá de Henares, Madrid, Spain. He is a Reviewer for several IET publications. His research activities are in the area of radar signal processing and advanced radar systems and concepts. Specifically, his interest focuses on high-resolution inverse synthetic aperture radar images and the design and validation of radar systems for healthcare applications.

Dr. Muñoz-Ferreras is a reviewer for several IEEE publications. He serves as a member of the Technical Review Board for the IEEE International Geoscience and Remote Sensing Symposium and the IEEE Radar Conference.

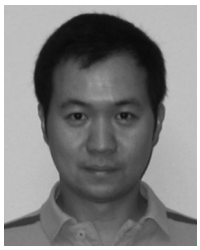

Changzhan Gu (S'07–M'13) received the B.S. and M.S. degrees in information and electronic engineering from Zhejiang University, Hangzhou, China, in 2006 and 2008, respectively, the M.S. degree in electrical engineering from the University of Florida, Gainesville, FL, USA, in 2010, and the Ph.D. degree in electrical engineering from Texas Tech University, Lubbock, TX, USA, in 2013.

He is currently a Senior RF Systems Engineer with MaxLinear Inc., Irvine Design Center, Irvine, CA, USA. His research interests include broadband RF systems, RF system-on-chip (SoC), wireless sensing technologies, and the biomedical applications of RF/microwaves.

Dr. Gu was the recipient of five Best Paper Awards as an author/coauthor of IEEE RWW 2011, 2012, and 2013 and IEEE WAMICON 2011 and 2012. He was the recipient of the IEEE Microwave Theory and Techniques Society (IEEE MTT-S) 2013 Graduate Fellowship for Medical Applications, 2013 Texas Tech Horn Professors Graduate Achievement Award, and 2012 Chinese Government Award for Outstanding Self-Financed Students Abroad.

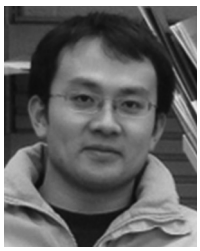

Changzhi Li (S'06–M'09–SM'13) received the B.S. degree in electrical engineering from Zhejiang University, Hangzhou, China, in 2004, and the Ph.D. degree in electrical engineering from the University of Florida, Gainesville, FL, USA, in 2009.

In the summers of 2007–2009, he was with Alereon Inc., Austin, TX, USA, and Coherent Logix Inc., Austin, TX, USA, where he was involved with ultra-wideband (UWB) transceivers and software-defined radio. In August 2009, he joined Texas Tech University, Lubbock, TX, USA, as an Assistant Professor. His research interests include biomedical applications of microwave/RF, wireless sensors, and RF/analog circuits.

Dr. Li was the Technical Program Committee (TPC) co-chair for IEEE WAMICON 2012 and 2013. He was the recipient of the National Science Foundation (NSF) Faculty Early CAREER Award in 2013, the Texas Tech Alumni Association New Faculty Award in 2012, and the IEEE Microwave Theory and Techniques Society (IEEE MTT-S) Graduate Fellowship Award in 2008. He was the finalist of the Vodafone Wireless Innovation Project competition in 2011. He was the recipient of seven best Conference/Student Paper Awards as author/advisor of IEEE Radio and Wireless Week (RWW) and the IEEE Wireless and Microwave Technology Conference (WAMICON).

Roberto Gómez-García (S'02–M'06–SM'11) was born in Madrid, Spain, in 1977. He received the Telecommunication Engineer and Ph.D. degrees in electrical and electronic engineering from the Polytechnic University of Madrid, Madrid, Spain, in 2001 and 2006, respectively.

Since April 2006, he has been an Associate Professor with the Department of Signal Theory and Communications, University of Alcalá, Alcalá de Henares, Madrid, Spain. For several research stays, he has been with the C2S2 Department, XLIM Research Institute (formerly IRCOM), University of Limoges, Limoges, France, the Telecommunications Institute, University of Aveiro, Aveiro, Portugal, and the Microwave Technology Branch, U.S. Naval Research Laboratory (NRL), Washington, DC, USA. He is an Associate Editor for IET MICROWAVES, ANTENNAS AND PROPAGATION. He was a Guest Editor for the 2013 Special Issue on "Advanced Tuneable/Reconfigurable and Multi-Function RF/Microwave Filtering Devices" of the IET MICROWAVES, ANTENNAS AND PROPAGATION. He is a Reviewer for several IET, EuMA, and Wiley journals. His current research interests are in the design of fixed/tunable high-frequency filters and multiplexers in planar, hybrid and monolithic microwave integrated circuit (MMIC) technologies, multi-function circuits and systems, and software-defined radio and radar architectures for telecommunications, remote sensing and biomedical applications.

Dr. Gómez-García is an associate editor for the IEEE TRANSACTIONS OF MICROWAVE THEORY AND TECHNIQUES and the IEEE TRANSACTIONS ON CIRCUITS AND SYSTEMS—I: REGULAR PAPERS. He was a guest editor for the Special Issue on "Advanced Circuits and Systems for CR/SDR Applications" of the IEEE JOURNAL ON EMERGING AND SELECTED TOPICS IN CIRCUITS AND SYSTEMS. He is a reviewer for several IEEE publications. He serves as a member of the Technical Review Board for several IEEE and EuMA conferences. He is also a member of the IEEE MTT-S Filters and Passive Components (MTT-8), IEEE MTT-S Wireless Communications (MTT-20), and IEEE CAS-S Analog Signal Processing Technical Committees.